

Application of step potential electrochemical spectroscopy in pouch cell prototype capacitors

Forghani, M. & Roberts, A.

Author post-print (accepted) deposited by Coventry University's Repository

Original citation & hyperlink:

Forghani, M & Roberts, A 2021, 'Application of step potential electrochemical spectroscopy in pouch cell prototype capacitors', *Electrochimica Acta*, vol. 390, 138845.

<https://dx.doi.org/10.1016/j.electacta.2021.138845>

DOI 10.1016/j.electacta.2021.138845

ISSN 0013-4686

Publisher: Elsevier

© 2021, Elsevier. Licensed under the Creative Commons Attribution-NonCommercial-NoDerivatives 4.0 International

<http://creativecommons.org/licenses/by-nc-nd/4.0/>

Copyright © and Moral Rights are retained by the author(s) and/ or other copyright owners. A copy can be downloaded for personal non-commercial research or study, without prior permission or charge. This item cannot be reproduced or quoted extensively from without first obtaining permission in writing from the copyright holder(s). The content must not be changed in any way or sold commercially in any format or medium without the formal permission of the copyright holders.

This document is the author's post-print version, incorporating any revisions agreed during the peer-review process. Some differences between the published version and this version may remain and you are advised to consult the published version if you wish to cite from it.

Application of Step Potential Electrochemical Spectroscopy in Pouch Cell Prototype Capacitors

Marveh Forghani*, Alexander J. Roberts
Institute of Future Transport and Cities, Coventry University,
Coventry CV1 5FB, United Kingdom

* Corresponding author

email: marveh.forghani@coventry.ac.uk

ABSTRACT

Herein we demonstrate the application of the step potential electrochemical spectroscopy (SPECS) technique to evaluate the electrochemical behaviour of large prototype capacitor devices for the first time. SPECS is generally applied for deconvoluting different charge storage mechanisms such as capacitive and diffusional processes. This study showed the effectiveness of SPECS technique to characterise the electrochemical performance of prototype pouch cell and to obtain invaluable information, including instability of the cell such as leakage current, degradation of the electrochemical cell, and a shortage of electrolyte species at highest potentials. This study also showed that the behaviour of capacitive and diffusional processes throughout different sweep rates is the same regardless of cell footprint and capacitance.

Keywords: Step potential electrochemical spectroscopy (SPECS), Electrochemical capacitors, Pouch cell, Prototype, High power

1. INTRODUCTION

Electrochemical energy storage and conversion technologies play a substantial role in contemporary society and meet the demands of various electronic systems with their effective cost, efficient energy storage and power delivery [1, 2]. Increasing demands for a more sustainable energy system has led to an interest in renewable forms of energy generation, such as solar, wind, tidal and geothermal energy [3-5]. However, electrochemical energy storage devices are essential to enable consistency of energy output of renewable technologies before transferring them to the grid system due to their intermittent nature [6-8]. Moreover, considerable effort is ongoing globally to develop and improve electric and hybrid-electric cars, which will not succeed without the development of more efficient electrochemical energy storage systems [9], also achieving improvements in electronic and portable small-scale devices dependent on increasing the energy and power density of their electrochemical energy storage systems [10, 11].

Electrochemical capacitors, batteries and fuel cell are three common categories of electrochemical energy storage and conversion technologies [12]. Electrochemical capacitors are known for their high power density and excellent cyclability [13-15], while fuel cells demonstrate high energy density and low power density [16]. Batteries typically exhibit higher energy density than electrochemical capacitors and higher power density than fuel cells [17].

This study focuses on the electrochemical performance of electrochemical capacitors. Commercial EDLCs or supercapacitors have been used in various sectors, including renewable energy, electronics, automotive and transportation, industrial and military [18]. The current principle applications of supercapacitors are in wind farms (pitch control and feathering of blades) [19], cranes and elevators (energy recovery, particularly in Gantry cranes for improved emissions and fuel economy) [20, 21], and in buses for public transport [22]. Future potential

applications under developments include those in electric vehicles [23, 24], implemented medical devices [25], satellite/space [26], and integrated powering of gas sensor [27].

The electrochemical capacitors exhibit by excellent power density ($\sim 10^3$ to 10^4 W.kg⁻¹) and cyclability ($>10^6$ cycles) [12-14]; however, their maximum energy density is relatively low (~ 12 Wh.kg⁻¹) [9, 15, 16]; as a result, considerable research and development have been undergoing around the world to enhancing the energy density of electrochemical capacitors [28]. Typically, the focus of these studies is on the development of advanced materials and electrolytes to increase energy density [29, 30]. Also, the majority of this research has been carried out at small scales such as Swagelok and coin cells. The study of electrochemical capacitors at small scales is essential for research and design, which has many benefits, including being cost-effective and easily accessible and requiring small amounts of material. These small format cells do not necessarily give the full picture as to performance in actual devices with issues arising due to the excess of electrolyte used, cell engineering and components, power capabilities and device lifetime.

Regardless of the electrode materials, electrolytes, and the size and type of electrochemical cells, it is often the aim to determine the electrochemical performance of the electrochemical system. In this regard, several electrochemical characterisation techniques can be applied to examine the performance of electrochemical systems. Whilst many of the methods and tests utilised are applied across both small electrochemical devices such as coin cells and larger prototype devices, differences exist in the interpretation and utilisation of the data produced. Techniques such as cyclic voltammetry (CV), galvanostatic charge-discharge (GCD) cycling [31-35] and electrochemical impedance spectroscopy (EIS) [36, 37] are used commonly to characterise the performance of small size electrochemical devices, and can provide valuable information about the electrochemical performance of electrode materials and electrolytes. For larger format prototypes and devices, such techniques are also employed but with an emphasis

on device specific (rather than material specific) parameters, true energy and power densities and lifetime assessed through extended float testing rather than cycling [37].

In this study, the step potential electrochemical spectroscopy (SPECS) technique which was recently developed and demonstrated as an effective method for studying electrochemical capacitors [38], has been applied to evaluate the electrochemical performance of prototype pouch cell capacitors. It has already been shown that the SPECS method is a highly effective technique to characterise the electrochemical behaviour of different electrode materials, including carbons and metal oxides [39, 40]. This method is based on applying a series of equal magnitude potential steps on a cell, with sufficient rest time to allow for equilibrium to be established for each step throughout an applied potential window. This slow sweep rate enables an electrode to approach its maximum charge storage capabilities. Moreover, it allows separation of charge storage mechanisms, such as electrical double layer and diffusion-limited processes [41, 42]. This technique has the potential to characterise the kinetic behaviour of the electrochemical cell over a full range of sweep rates [43] and also to provide additional information about the existence of the residual current such as leakage and self-discharge current, the stability of electrode materials, the ionic mobility of various electrolyte species, the equivalent series resistance of the electrode materials and the effectiveness of the engineering of the device [44-46]. The SPECS method has also been used for deconvoluting different charge storage mechanisms such as capacitive and diffusional processes in electrochemical energy storage technologies [43].

In this study, we investigated for the first time the application of the SPECS method in full prototype pouch cells of over 100 F. Through the application of the SPECS technique, new insight has been gained in performance at the device scale, the role of cell components and engineering aspects and also further insight into electrode and electrolyte requirements.

2. EXPERIMENTAL

2.1. Electrode and Pouch Cell Preparation

Electrodes were prepared by roll-to-roll coating of the water-based inks of YP50-F activated carbon (Kuraray, Japan), C65 carbon black (Imerys, UK) conductive agent, and binders carboxymethyl cellulose (CMC, Dai Ichi, Japan) and styrene butadiene rubber (SBR, Zeon Europe) in a ratio of 89:5:6 (active: conductive additive: binders). The inks were coated onto etched aluminium current collector (K-JCC, Korea) and then calendered to give electrodes of total mass loading 60 gm^{-2} . The double-sided electrodes were then cut and stacked, and assembled using pouch cell prototyping line (MTI Corporation, USA), before being dried in an argon glove box and filled with 1 M tetraethylammonium tetrafluoroborate (TEABF_4) (Sigma-Aldrich) in acetonitrile (99.99 %; Sigma-Aldrich) under argon environment with subsequent pouch cell sealing.

In this study, six pouch cells were made to observe the influence of different cell geometric size and capacitance. The specifications of these pouch cells are shown in Table 1.

2.2. Experimental Protocol

In this study, a VMP3 Potentiostat (BioLogic) was used to run the electrochemical experiments. Initially, each pouch cell was cycled with a constant current of 5 A in the range of 1.35 to 2.7 V for 50 cycles. In the first series of experiment, three electrochemical cells shown in Table 2, were cycled at a sweep rate of 25 mV.s^{-1} between 0 to 2.7 V. The galvanostatic charge-discharge (GCD) test was also applied to identify the capacitance and ESR, at the constant current of 1 A in the potential window of 0 to 2.7 V. The cells were further characterised for rate and power characteristics through constant current cycling to a maximum of 50 A and also constant power cycling between 50 and 2500 W Kg^{-1} (based on fully packaged device mass), both between V_{max} and $V_{\text{max}}/2$. This was followed by the SPECS experiment with a 30 mV potential step and 1800 s equilibration time. In the SPECS experiment from the minimum

potential (0.0 V), a series of equipotential 30 mV steps were applied to the electrochemical cell. At each potential step, the cell was allowed to equilibrate for a certain step time of 1800 s before applying the next potential step. This procedure was continued until a full range of the potential window (0.0 V to 2.7 V) was covered. The process was then reversed from the maximum potential of 2.7 V to the minimum potential of 0.0 V. The current response to each potential step was recorded as a function of time until one entire charge/discharge cycle was completed. In the second series of experiments, three electrochemical cells given in Table 3 underwent the float test. Initially, the GCD test at the constant current of 1 A in the potential window of 0 to 2.7 V was applied to measure the capacitance and the ESR of the electrochemical cells before the float test. This was followed by the SPECS experiment with the same experimental protocol mentioned above. Then, the electrochemical cells were held at 2.7 V for 200 hours. The GCD and SPECS experiments with similar experimental parameters were then carried out for the second time in order to measure the degradation processes after the float test.

3. RESULTS AND DISCUSSION

3.1. Galvanostatic Charge-Discharge and Constant Power Tests

The capacitance and ESR of the pouch cells were obtained from GCD test at the constant current of 1 A in the potential window of 0 to 2.7 V. The results of this test have been given in Table 2. The small pouch cell 2 (SPC2) has the highest capacitance of ~ 120 F and the lowest ESR of 7.1 m Ω . It can be seen that by increasing the surface area of the electrodes, the capacitance increases while the ESR decreases. The rate behaviour of the cells can be seen in Figure 1, with little change observed over the wide range of currents employed. It is noted that for small pouch cell 1 (SPC1), the maximum current utilised was limited to 40 A due to its lower capacitance. The Ragone plot for the cells tested is shown in Figure 2. All cells showed

expected excellent power performance with a gravimetric energy density of ca. 4 Wh Kg⁻¹ maintained at a power density of 500 W Kg⁻¹, and 2.2 – 2.7 Wh Kg⁻¹ at 2500 W Kg⁻¹.

3.2. Step Potential Electrochemical Spectroscopy (SPECS) Characterisation

3.2.1. Contributions

In the SPECS method, a current is measured as a function of time at each potential step over the full potential window. The SPECS current is a result of the diffusion-limited processes and the electrical double layer at the surface and bulk of the electrode. The fast and facile electrical double layer or capacitive charging process can occur at the geometric surface area of the electrode as well as the surface of the pores in the bulk of the electrode. The capacitive current (i_C ; A), in a simple RC circuit, when applying a potential step of E (V), is given by [47]; i.e.,

$$i_C = \frac{\Delta E}{R} \exp\left(-\frac{t}{RC}\right) \quad \dots(1)$$

where R (Ω) is the series resistance, t (s) is the time, and C (F) is the capacitance of the electrical double layer.

The diffusion-limited process is much slower than the electrical double layer processes due to continuous redox reactions. Therefore, the diffusional current decreases slowly over the extended equilibration time. This current (i_D ; A) can be modelled using the Cottrell equation for semi-infinite planar diffusion [47]; i.e.,

$$i_D = nFAC \left(\frac{D}{\pi t}\right)^{1/2} = \frac{B}{t^{1/2}} \quad \dots(2)$$

Where n is the number of electrons involved in an electrode reaction, F is Faraday's constant (96496.7 C/mol), A (m^2) is the electrode area, D (m^2/s) is the diffusion coefficient of the species, C is the concentration of the species at the surface of the electrode (mol/m^3), and B is proportional to the capacitance of the diffusion-limited process C_D (F).

It is expected that the SPECS current reaches zero at the end of the equilibration time, but in reality, this does not happen due to the existence of some residual processes, alongside capacitive and diffusion-limited processes that do not equilibrate by the end of the equilibration time. The residual processes probably occur due to slow diffusional processes in a given equilibration time. Hence, the residual current (i_R ; A) is another term that needs to be added to the SPECS model to account for the total current.

Thus, the SPECS model consists of the electrical double layer or capacitive current at the geometric and porous surface areas and the current related to the diffusion-limited process and residual process. The total current of SPECS data can be given by; i.e.,

$$i_T = i_{C1} + i_{C2} + i_D + i_R \quad \dots(3)$$

where i_{C1} and i_{C2} are capacitive currents at the geometric and porous surface areas, respectively.

3.2.2. Deconvolution of the SPECS current

The electrochemical cells were subjected to the SPECS experiment after being conditioned by constant current cycling. Before starting the SPECS experiment, the cells were equilibrated at 0 V potential. A series of anodic 30 mV potential steps were applied to the cell with 30 min equilibration time between each step, to an upper potential limit of 2.7 V.

Subsequently, a series of cathodic potential step with the same magnitude were applied back down to the lowest potential limit of 0 V to cover a full cycle of charging and discharging.

Figure 3(a) shows full current spikes for the SPECS experiment resulting from each of the individual potential steps during one cycle of charging/discharging with the staircase corresponding potential step profile overlaid. It is evident that the current spikes vary over the potential window, which indicates the potential dependent of charge storage mechanisms. The theoretical SPECS data then was fitted to each individual experimental i-t transient using linear least squares regression. Figure 3(b) shows an expanded view of individual current response (i-t transient) and its corresponding predicted currents from SPECS model as per Eqn(3) for the anodic 30 mV step to the cell potential of 1.35 V. Also, the inset shown here is a plot of differences between the experimental data and predicted current.

The contributions from the geometric and porous capacitive processes, diffusional process and residual process can be seen in Figure 3(b). The electrical double layer or capacitive process is a dominant charge storage mechanisms for active materials such as activated carbon in organic electrolyte. The electrode used in this study is highly porous. In reality, the actual capacitive process is more complicated as some pores are highly accessible to the electrolyte and some pores with smaller pore size or within the bulk of the electrode are less available to the ions in the electrolyte. In this study, the outer surface of the electrode and pores with more accessibility to the electrolyte ions refer as a geometric surface area. While the smaller pores and pores within the bulk of the electrode material considered as a porous surface area. However, it should be mentioned that the boundary between the geometric surface area and porous surface area is not well defined and is dependent on potential, nature of the pores and also electrolyte properties. In the SPECS model, the same equation is used for the two capacitive processes, but they can be distinguished from their different time constant. It is evident that the time constant for the geometric capacitive process is much lower than the one for the porous capacitive process, as in the latter case, ions need more time to reach and occupy the surface of the inner surface areas. The peak in current occurs as a result of the fast and facile geometric

capacitive process, which is the result of the immediate gathering of the ionic charges at the electrode-electrolyte interface as soon as the potential step is applied. However, Figure 3(b) shows that this current decays quickly almost after 5 s from applying the 30 mV potential step as a result of equilibration of the electrical double layer processes at the geometric surface area. The current resulting from the porous capacitive process is the second significant current which dissipated slightly longer in almost 10 s due to the slower response of ion association and dissociation in the less accessible pores.

Diffusion-limited process in the organic activated carbon system could be associated with the mass transport of electrolyte ions within the pores of the activated carbon. It is evident in Figure 3(b) that the contribution of the diffusional process is minimal.

The residual current can be an indicator of instability in the electrochemical system, and it could represent the kinetically slow redox processes over the course of equilibration time at the end of each potential step. The origin of these side redox reactions in carbon-based electrodes in the organic medium is believed to have a number of possible sources, including the consumption of an electroactive species at the surface and bulk of electrode, the presence of water, molecular oxygen and impurities in the organic salt. These impurities, which can cause ongoing redox reactions, have been previously observed using a sensing electrode [45, 48]. In a short period of equilibration time (~ 1 min), the contribution of the residual current is insignificant; however, at longer times when eventually other processes decayed to zero, it becomes more significant due to its non-zero constant current.

3.2.3. Parameter Outputs from SPECS Analysis

The experimental currents obtained at each individual potential step was deconvoluted to the capacitive current at the geometric and porous surface areas, diffusional and residual currents using the SPECS model. Figures 4 (a)-(d) show the parameter outputs obtained by the linear

least-squares regression analysis for each individual current resulted at the particular potential step throughout the potential window during charging and discharging processes, including the geometric capacitance (Figure 4(a)), porous capacitance (Figure 4(b)), geometric and capacitive time constant (Figure 4(c)), and diffusional and residual processes (Figure 4(d)). It should be mentioned that all three cells showed similar behaviour; hence only the parameter outputs of small pouch cell 1 (SPC1) is presented in Figures 4 (a)-(d). These results indicate the characteristics of the whole cell, including the active material, binder, the conductive network, current collector properties, electrolyte properties, welding and engineering of the cell. It is interesting to note the following points for this data:

- (i) As it was mentioned before, the boundaries between the geometric and porous capacitive processes are not well defined, and these processes are distinguished by their different time constant. It can be seen that the time constant for the geometric capacitive process, which is in a range of 0.3 to 0.8 s, is much lower than the time constant of the porous capacitive process with a range of 1 to 5 s. The geometric capacitance is a dominant charge storage mechanisms at most of the anodic and cathodic potential scan in the potential range of 0 V to almost 1.75 V. Figure 4(a) shows a dramatic decrease in the geometric capacitance heading towards the anodic potential limit of 2.7 V. While the porous capacitance is a dominant capacitive process at the higher extremes of the potential window examined.
- (ii) The changes in the geometric and porous resistance during charging and discharging processes are associated with the changes of the series resistance of the electrode material, and the cell resistance is expected to remain constant with a relatively low value (less than 9 m Ω) during the entire process.
- (iii) During the charging process, the geometric capacitance slightly increased while the geometric resistance remained constant at the low value of 10 m Ω . However, the

geometric resistance dramatically increased when approaching the anodic potential limit. As a result, the geometric capacitance sharply decreased towards the upper potential limit. This opposing behaviour was also observed during the cathodic scan when the geometric resistance started to decrease at the upper potential limit of 2.7 V, which led to increasing geometric capacitance. Overall the changes in the geometric resistance remained small (10 to 50 m Ω). In contrast, the geometric capacitance showed a variation of almost 80 F during the anodic and cathodic scan, respectively. As a result, the changes in the geometric time constant is more governed by the geometric capacitance.

- (iv) The behaviour of the porous capacitive process is shown in Figure 4 (b), which is almost the opposite of the geometric capacitive process. During the anodic scan, the porous resistance decreased dramatically by increasing the potential step towards the upper potential limit. At the same time, the porous capacitance remained almost constant at the low value of 10 to 15 F during this sharp dropping in resistance. Eventually, the porous resistance reached the low resistance value of 10 m Ω at the potential of 2 V, and it remained constant for the rest of the anodic scan. As soon as the porous resistance reached the lower values, the porous capacitance sharply increased by increasing the potential steps towards the maximum cell potential. It should be mentioned that while the capacitance was increasing during the anodic scan for the porous processes, it was decreasing for the geometric processes. This indicates that increasing the potential step increases the driving force to insert the ions into the bulk of the electrode materials. The surge of ions into the bulk of the electrode could increase the ionic conductivity, and eventually decreasing the series resistance of the electrode and increasing the porous capacitance. During the cathodic scan, the opposite behaviour can be observed as by increasing the porous

resistance, the porous capacitance decreased. At the lower potentials, the resistance of inner porous surfaces has higher values due to the lower driving force to insert ions into the inner surface areas. The changes in the porous resistance are significant during the charging and discharging processes which are in the range of 10 to 1100 m Ω . Hence the porous time constant is more influenced by the porous resistance.

- (v) At higher potentials, the porous capacitance is a dominant charge storage process implying that the ionic species are drawn mostly to the inner porous surface areas. Hence the dramatic decrease in the geometric capacitance at higher potentials could be an indication of the shortage of ions in the electrolyte to occupy all pores of the activated carbon. This dramatic decrease of geometric capacitance at high potentials is in contrast with the results from small cells such as the Swagelok cell which there is an abundant of ions in electrolyte [49].
- (vi) Figure 4(d) shows the changes in diffusional parameter throughout the charging and discharging processes. The diffusional parameter slightly increased, heading towards the anodic and cathodic potential limits; however, its changes are minimal. Generally, the diffusional processes rise at high cell potentials due to the greater driving force, which can lead to the higher mass transport of ions into the bulk of the electrode.
- (vii) The variations in the residual current are also shown in Figure 4(d). Overall the residual current is so insignificant, and its maximum value is less than 3 m Ω . The residual current gradually increased during the anodic scan. Still, then it sharply increased at the extremes of the potential window examined. This behaviour is expected as the residual current could be an indicator of expected ongoing degradation processes during the anodic scan. Also, it indicates instability of the cell at high potential due to a slow degradation mechanism. The opposite fashion

can be observed during the cathodic scan, decreasing the current by decreasing the potential step.

3.2.4. Synthetic Voltammetry

Parameter outputs from the SPCEs analysis can be used to generate a series of synthetic voltammograms for each charge storage contribution at different relative sweep rates. To do so, the current response for an individual i-t transient is averaged out to each specific time that current data was collected after that potential step. In fact, each specific time corresponds to a relative sweep rate, which can be calculated by dividing the potential step size (in this case, 30 mV) over that specific time. For instance, the specific time of 0.2 s after the potential step is corresponding to the relative sweep rate of 150 mV.s⁻¹. Hence, for each individual i-t transient, the current can be averaged over a range of different relative sweep rates.

It should be mentioned that the average currents of the capacitive, diffusional and residual processes should be calculated in different manners based on their nature. Firstly, it should be considered that the capacitive process at each potential step is independent of the capacitive processes at previous potential steps. This is due to the fast accumulation of ions at the electrode-electrolyte interface, which means that the completion of the capacitive process at each potential step occurs before initiating the subsequent potential step. Hence, the timing of the individual i-t transient can be shifted according to the required rate (for instance, 2 s), which leads to overlapping the i-t transient responses from multiple potential steps at the same time. Therefore, the average current from each of overlapping i-t transients within the step timeframe can be calculated [49] i.e.,

$$i_{TOT} = \sum_{n=1}^n i_{ave,n} = \sum_{n=1}^n \frac{\Delta EC_n}{\Delta t} \left\{ \exp\left(-\frac{t_n}{R_n C_n}\right) - \exp\left(-\frac{t_{n+1}}{R_n C_n}\right) \right\} \quad \dots(4)$$

where $i_{ave,n}$ is the average current flowing from the n^{th} overlapping i-t transient, R_n and C_n are the resistance and capacitance of the n^{th} step, and $\Delta t = t_{n+1} - t_n$ which is the shifted time base on the SPECS analysis.

Conversely, diffusional processes are much slower in nature than the capacitive processes due to the slower kinetics associated with the intercalation of species into the bulk of electrode and pores. Hence, the current response from diffusional processes continuous over the full range of equilibration time and is dependent on preceding steps.

It should be mentioned that for diffusional processes, the dependence on previous potential steps is inherent in the measured data, so unlike summing the average current across all potential steps for the capacitive process, the average current (i_{ave} ; A) for diffusional processes, in each individual step, is obtained [49] i.e.,

$$i_{ave} = \frac{q}{t} = \frac{B}{t} \int_0^t t^{-1/2} dt = \frac{2B}{t^{1/2}} \quad \dots(5)$$

where q is the charge (C) out to the time base of the analysis (t ; s), B is the diffusional parameter obtained by Eqn (2).

The residual process also is a slow process, and like a diffusional process, its current response is dependent on previous steps. The residual current is constant at each potential step, and these constant values are used to calculate the average current of the residual process in each individual step throughout the potential window. Eventually, the total average current can be obtained by summing the average currents of all contributions at each potential step.

After calculating the average current for different contributions, a synthetic voltammogram for the total average current as well as each charge storage mechanisms can be generated at different relative sweep rates. The comparison between the experimental CV data and synthetic voltammograms generated from the SPECS analysis at the sweep rate of $25 \text{ mV} \cdot \text{s}^{-1}$ for the big

pouch cell 1 (BPC1) is shown in Figure 5. It can be seen that there is good agreement between the shape of the experimental voltammetric data and that extracted from the SPECS analysis. However, the SPECS analysis slightly indicates the higher voltammetric current in both anodic and cathodic scans implying that the SPECS method can determine the full capacity of the cell due to the long equilibration time between each potential step (in this case, 1800 s). The synthetic voltammogram of the geometric capacitive process has the main contribution up to almost 2 V, then its position replaced by the porous capacitive process to the higher cell potentials. The dramatic decrease in the geometric capacitive current at higher potentials could be an indication of the shortage of ions in the electrolyte to occupy all pores of the inner surface areas. This is in contrast with the synthetic voltammogram of capacitive processes for small cells in which there is an abundant of ions in electrolyte [43, 44, 49]. The diffusional and residual processes have a negligible contribution at the relative sweep rate of 25 mV.s⁻¹.

3.2.5. Cell Capacitance and Cell behaviour

The synthetic voltammograms generated from the SPECS analysis then can be used to determine the capacitance as a function of sweep rate. The conventional approach to calculating the capacitance from CV data can be applied to determine the capacitance of the synthetic voltammograms from the SPECS data [47]; i.e.,

$$C = \frac{q}{\Delta E} = \frac{1}{v\Delta E} \int_{E_i}^{E_f} idE \quad \dots(6)$$

where C is the capacitance (F), q is the capacity (C), ΔE is the potential window (= E_f – E_i; V), and v is the sweep rate (V.s⁻¹).

Figure 6 contains the cathodic capacitances as well as the percentage contribution made by each component as a function of sweep rate for the three pouch cells being studied. The overall capacitance of small pouch cell 1 (SPC1) with the smaller active mass is lower than the other

two cells with the same mass. However, the behaviour of various contributions made to the overall performance is the same for all three cells. The total capacitance increases by decreasing the sweep rates. This could be due to the increasing the capacitance of slow processes such as diffusional and residual current at lower scan rates in addition to the capacitance of capacitive processes. At lower sweep rates, there is more time for ions to diffuse into the bulk of the electrode, which leads to an increase in total capacitance. The capacitance of the geometric capacitive process dominates throughout the full range of sweep rates, and its value almost remains constant. The capacitive capacitance at the porous surface area is also significant and mainly remains constant through the full range of sweep rates with slightly decreasing at the highest sweep rate. The reason is the ions have less time to accumulate at the inner porous surface areas by increasing the rate of potential sweep rate. The reduction in the porous capacitive capacitance at the highest sweep rate also leads to the decreasing in the total capacitance as other contributions almost remain constant. Overall the capacitance of diffusional and residual processes is insignificant through the entire range of sweep rates. However, as the sweep rate decreases, the contribution made by both diffusional and residual processes increases, which leads to an increase in the capacitance gradually. Of course, this was to be expected given the slow kinetics and diffusion rate associated with these processes

To supplement this analysis, Figures 6(b, d, f) shows the percentage contribution made by each process. The contribution of the geometric process increases by increasing the sweep rates, and at low sweep rates, the contribution of the diffusional and residual current increases exponentially. The contribution of the porous capacitive process is almost constant through the full range of sweep rates. Here, the nature of these processes governs their contributions at different scan rates. For kinetically slow processes such as diffusional and residual currents, ions need more time to penetrate and diffuse through the inner bulk of electrode materials, so at low sweep rates, the contribution of these processes increases. Conversely, for the fast and

facile capacitive processes, ions can accumulate at the interface of electrode-electrolyte in a fraction of seconds, so at higher scan rates, the major contributions are the capacitive processes. Also, as it is expected at a very high scan rate, the contribution of the geometric process increases while the porous capacitive contribution slightly decreases. The reason is by increasing the sweep rates, the inner pores are less accessible to the ions. Also, this result is in agreement with the time constant values shown in Figure 4(c), as the time constant of porous surface area or less accessible surfaces is much greater than the time constant of the geometric surface area or more free surfaces. Also, the effect of different geometric size and capacitance on the overall behaviour of the pouch cell can be seen here. It is assumed that the charge storage mechanisms (capacitive and diffusional processes) would be the same for various type of organic electrolytes; however, the current response and contributions associated with the charge storage mechanisms would vary due to the different ion and counter ion sizes and ionic conductivity. Also, it is expected that the carbon texture, particularly pore size distribution, would affect the contributions of various charge storage mechanisms. The comparison of three pouch cells indicates that the cell footprint and capacitance have a negligible effect on the behaviour of various contributions over the full range of the sweep rates.

3.3. The Influence of Float Test on Cell Behaviour

3.3.1. Galvanostatic Charge-Discharge Pre and Post Float Test

In the second part of this study, the GCD tests were applied to three pouch cells before and after conducting 200 hours float test at 2.7 V. The capacitance and ESR obtained from the GCD test at the constant current of 1 A in the potential window of 0 to 2.7 V are given in Table 3. The influence of the float test on the performance of the pouch cells is evident. Overall, the total capacitance decreased 3 to 5% and, the ESR increased 9 to 12% after conducting the float test.

3.3.2. *SPECS Analysis Pre and Post Float Test*

The SPECS method was applied before and after conducting the float test to observe changes in pouch cells performances. The parameter outputs from the SPECS analysis has been obtained in the same manner described in Section 3.2.3. It should be mentioned that all three cells (BPC2, BPC3, & BPC4) showed closely similar behaviour; hence only the parameter outputs of big pouch cell 2 (BPC2) is presented in Figures 7 (a)-(d). The comparison between the time constant at the geometric surface area before and after the float test is shown in Figure 7(a). The lower time constant indicates the easier accessibility of the ions to the pores. It can be seen that the shape of the pre-float and post-float test graphs is similar, and it drops dramatically towards higher potentials due to the greater electrochemical driving force, which facilitates the ion movement. Figure 7(b) shows the comparison of pre- float and post-float test time constant at the porous surface area, which is less accessible to the ions. It is evident that the porous time constant significantly decreased at lower potentials after the float test. This is believed to be a result of improved wettability as a result of further conditioning and degradation. However, at higher potentials, the wettability of the pores does not have too much impacts on the porous time constant due to the higher electrochemical driving force. Hence, the pre-float and post-float test time constants at the porous surface areas are similar at higher potential. Figure 7(c) compares the diffusion parameters before and after the float test. It can be seen that the diffusion parameter increased at lower potentials. Again, this is believed to be a result of improved wettability and possibly a consequence of the loss of some deep/hard to access porosity to the electrolyte species due to degradation mechanisms and/or ion entrapment. The diffusion parameters are similar for both pre-float and post-float test graphs at higher potentials due to the higher electrochemical driving force of ions. The most interesting graph is the comparison of the residual currents for the pre-float and post-float test, which is given in Figure 7(d). The residual current graphs for the pre-float and post-float test are similar

for the entire potential window, except at the highest cell potential. It is evident that the residual current before conducting the float test increased dramatically at the highest cell potential and also decreased after completing the float test. As mentioned earlier, the residual process is an indicator of instability in the electrochemical system and could result from side redox reactions, including the consumption of an electroactive species at the surface and bulk of electrode, the presence of water, molecular oxygen and impurities in the organic salt. Although it would be expected that the degradation of the electrodes during the float test increases the residual current, by holding the cell at 2.7 V potential for 200 hours, these side reactions and impurities gradually can be consumed and declined over time. Thus, after the float test, the decay in the residual current at the highest cell potential can be observed.

The overall capacitance and contribution of different processes, including the capacitive processes at the geometric and porous surface areas, diffusional and residual processes, for three pouch cells of BPC2, BPC3 and BPC4 have been obtained in a similar way presented in Sections 3.2.4 and 3.2.5, and the results graphs are given in the Supplementary Material Figures SM 11 and SM 12. The results indicate that the capacitance at the geometric surface areas is slightly higher post-float test due to the wettability and further conditioning of the electrochemical cells during the float test. However, there is a significant decrease in the capacitance at the porous surface area after conducting the float test. This could be the results of blocking the inner pores during the float test. At lower sweep rates, the diffusional capacitance increases after conducting the float test, which could be the results of the wettability of the inner pores of the electrode. Also, the contribution of the residual process increases after the float test, indicating the degradation of electrochemical cells during the float test. Overall, the total capacitance of the electrochemical cells decreases after the float test throughout the full range of sweep rates except at the very low sweep rate.

4. CONCLUSIONS

Herein the application of the step potential electrochemical spectroscopy (SPECS) method in large prototype pouch capacitors is demonstrated for the first time. Prototype pouch cells with different geometric sizes and capacitance were examined. The pouch cells were made of activated carbon electrode with the organic electrolyte of 1 M TEABF₄ in ACN. The SPECS method deconvoluted the current resulted at each individual potential step into various contributions, including the capacitive processes at the geometric and porous surface areas and the diffusional and residual currents.

The outcome of this study indicates that the geometric capacitive process is a dominant contribution through the full range of sweep rates. At a high cell potential, the capacitance of the porous capacitive process increased while the capacitance of the geometric capacitance decreased, indicating the shortage of ions in the electrolyte at higher potentials. This is in contrast with the behaviour of geometric capacitive process for small cells such as Swagelok cell which there is an abundant of ions in the electrolyte. The contribution of the diffusional process remained insignificant at higher sweep rates. Still, it increased at lower sweep rates as ions have more time to diffuse through the bulk of the electrode. The contribution of residual current, which is an indicator of instability in the electrochemical system, increased at lower sweep rates. The residual process is a kinetically slow process which could be a result of ongoing redox reactions of impurities in the electrolyte. Also, the residual current dramatically increased at the highest cell potential indicating the instability and degradation of the cell at higher potentials. Overall, the total capacitance of the pouch cell increased by decreasing the sweep rates due to the increase in contributions of slow processes such as diffusional and residual processes. All pouch cells showed similar behaviour over the full range of sweep rates regardless of their varied footprint and capacitance.

Moreover, the SPECS method was applied to the second series of pouch cells before and after conducting the float test for 200 hours at the maximum cell potential of 2.7 V. After the float test, the decay in the residual current at the highest cell potential has been observed. This could be the results of the consumption of impurities over time. At lower potentials, the shorter capacitive time constant was observed after the float test, which is believed to be the result of improved wettability as a result of further conditioning and degradation. However, after the float test, the contribution of the capacitive processes at the porous surface area was dramatically decreased over the full range of the sweep rates. This could be the results of blocking the inner pores during the float test. Overall, after conducting the float test, the total capacitance of the pouch cells decreased at most of the full range of sweep rates (higher than $0.0001 \text{ V}\cdot\text{s}^{-1}$).

ACKNOWLEDGEMENTS

The authors would like to thank the Materials Research Hub for Energy Conversion, Capture, and Storage (M-RHEX) (EP/R023581/1) for funding this work.

REFERENCES

1. Hall, P.J. and E.J. Bain, *Energy-storage technologies and electricity generation*. Energy policy, 2008. 36(12): p. 4352-4355.
2. Hall, P.J., Mojtaba Mirzaeian, S. Isobel Fletcher, Fiona B. Sillars, Anthony JR Rennie, Gbolahan O. Shitta-Bey, Grant Wilson, Andrew Cruden, and Rebecca Carter, *Energy storage in electrochemical capacitors: designing functional materials to improve performance*. Energy & Environmental Science, 2010. 3(9): p. 1238-1251.
3. Bull, S.R., *Renewable energy today and tomorrow*. Proceedings of the IEEE, 2001. 89(8): p. 1216-1226.
4. Balachandra, P., H.S.K. Nathan, and B.S. Reddy, *Commercialization of sustainable energy technologies*. Renewable Energy, 2010. 35(8): p. 1842-1851.
5. Kadiri, M., Ahmadian, R., Bockelmann-Evans, B., Rauen, W., and Falconer, R., *A review of the potential water quality impacts of tidal renewable energy systems*. 2012. 16(1): p. 329-341.

6. Andersen, A.N. and H. Lund, *New CHP partnerships offering balancing of fluctuating renewable electricity productions*. Journal of Cleaner Production, 2007. 15(3): p. 288-293.
7. Østergaard, P.A., *Transmission-grid requirements with scattered and fluctuating renewable electricity-sources*. Applied Energy, 2003. 76(1): p. 247-255.
8. Soloveichik, G.L., *Battery technologies for large-scale stationary energy storage*. Annual review of chemical and biomolecular engineering, 2011. 2: p. 503-527.
9. Miller, J. R., and Burke, A., *Electrochemical capacitors: challenges and opportunities for real-world applications*. 2008. 17(1): p. 53.
10. Lee, S.W., Gallant, B. M., Byon, H. R., Hammond, P. T., and Shao-Horn, Y., *Nanostructured carbon-based electrodes: bridging the gap between thin-film lithium-ion batteries and electrochemical capacitors*. 2011. 4(6): p. 1972-1985.
11. Xu, L. L., Guo, M. X., Liu, S., and Bian, S. W., *Graphene/cotton composite fabrics as flexible electrode materials for electrochemical capacitors*. 2015. 5(32): p. 25244-25249.
12. Simon, P. and Y. Gogotsi, *Materials for electrochemical capacitors*. Nature materials, 2008. 7(11): p. 845-854.
13. Frackowiak, E. and F. Béguin, *Carbon materials for the electrochemical storage of energy in capacitors*. Carbon, 2001. 39(6): p. 937-950.
14. Mombeshora, E.T. and V.O. Nyamori, *A review on the use of carbon nanostructured materials in electrochemical capacitors*. International Journal of Energy Research, 2015. 39(15): p. 1955-1980.
15. McCloskey, B.D., *Expanding the Ragone plot: Pushing the limits of energy storage*. 2015, ACS Publications.
16. Winter, M. and R.J. Brodd, *What are batteries, fuel cells, and supercapacitors?* 2004, ACS Publications.
17. Davies DM, Verde MG, Mnyshenko O, Chen YR, Rajeev R, Meng YS, Elliott G., *Combined economic and technological evaluation of battery energy storage for grid applications*. Nature Energy, 2019. 4(1): p. 42.
18. Sumangala TP, Sreekanth MS, Rahaman A., *Applications of Supercapacitors*. Handbook of Nanocomposite Supercapacitor Materials III: Selection, 2021: p. 367-393.
19. <https://www.skeletontech.com/wind-turbine-pitch-control>. Accessed 15/06/2021. .
20. <https://www.skeletontech.com/ultracapacitors-elevatorkers-jan>. Accessed 15/06/2021.

21. Kermani, M., et al., *Ultracapacitors for port crane applications: Sizing and techno-economic analysis*. *Energies*, 2020. 13(8): p. 2091.
22. Maher, B.J.B.P.P. and Technology, *Ultracapacitors provide cost and energy savings for public transportation applications*. *Power Products & Technology Magazine* [Online], 2006. 10(6).
23. Hannan, M., et al., *Review of energy storage systems for electric vehicle applications: Issues and challenges*. *Renewable and Sustainable Energy Reviews*, 2017. 69: p. 771-789.
24. Veneri, O., C. Capasso, and S.J.A.E. Patalano, *Experimental investigation into the effectiveness of a super-capacitor based hybrid energy storage system for urban commercial vehicles*. *Applied Energy*, 2018. 227: p. 312-323.
25. Mosa IM, Pattammattel A, Kadimisetty K, Pande P, El-Kady MF, Bishop GW, Novak M, Kaner RB, Basu AK, Kumar CV, Rusling JF. *Ultrathin graphene–protein supercapacitors for miniaturized bioelectronics*. *Advanced energy materials*, 2017. 7(17): p. 1700358.
26. Chin KB, Brandon EJ, Bugga RV, Smart MC, Jones SC, Krause FC, West WC, Bolotin GG. *Energy storage technologies for small satellite applications*. *Proceedings of the IEEE*, 2018. 106(3): p. 419-428.
27. Yadav AA, Lokhande AC, Pujari RB, Kim JH, Lokhande CD. *The synthesis of multifunctional porous honey comb-like La₂O₃ thin film for supercapacitor and gas sensor applications*. *Journal of colloid and interface science*, 2016. 484: p. 51-59.
28. Vangari, M., T. Pryor, and L. Jiang, *Supercapacitors: review of materials and fabrication methods*. *Journal of Energy Engineering*, 2012. 139(2): p. 72-79.
29. Borenstein, A., Hanna, O., Attias, R., Luski, S., Brousse, T., and Aurbach, D., *Carbon-based composite materials for supercapacitor electrodes: a review*. *Journal of Materials Chemistry A*, 2017. 5(25): p. 12653-12672.
30. Zhi, M., Xiang, C., Li, J., Li, M., and Wu, N., *Nanostructured carbon–metal oxide composite electrodes for supercapacitors: a review*. *Nanoscale*, 2013. 5(1): p. 72-88.
31. Fellows, H. M., Forghani, M., Crosnier, O., and Donne, S. W., *Modelling voltametric data from electrochemical capacitors*. *Journal of Power Sources*, 2019. 417: p. 193-206.
32. Forghani, M. and S.W. Donne, *Complications When Differentiating Charge Transfer Processes in Electrochemical Capacitor Materials: Assessment of Cyclic Voltammetry Data*. *Journal of The Electrochemical Society*, 2019. 166(8): p. A1370-A1379.

33. Kulkarni, S. B., Patil, U. M., Shackery, I., Sohn, J. S., Lee, S., Park, B., and Jun, S., *High-performance supercapacitor electrode based on a polyaniline nanofibers/3D graphene framework as an efficient charge transporter*. Journal of Materials Chemistry A, 2014. 2(14): p. 4989-4998.
34. Mai, L. Q., Minhas-Khan, A., Tian, X., Hercule, K. M., Zhao, Y. L., Lin, X., and Xu, X., *Synergistic interaction between redox-active electrolyte and binder-free functionalized carbon for ultrahigh supercapacitor performance*. Nature communications, 2013. 4: p. 2923.
35. Wee, G., Salim, T., Lam, Y. M., Mhaisalkar, S. G., and Srinivasan, M., *Printable photo-supercapacitor using single-walled carbon nanotubes*. Energy & Environmental Science, 2011. 4(2): p. 413-416.
36. Barsoukov, E. and J.R. Macdonald, *Impedance Spectroscopy: Theory, Experiment, and Applications*. 2005: Wiley.
37. Lu, M., F. Beguin, and E. Frackowiak, *Supercapacitors: materials, systems and applications*. 2013: John Wiley & Sons.
38. Dupont, M.F. and S.W. Donne, *A Step Potential Electrochemical Spectroscopy Analysis of Electrochemical Capacitor Electrode Performance*. Electrochimica Acta, 2015. 167: p. 268-277.
39. Dupont, M.F. and S.W. Donne, *Faradaic and Non-Faradaic Contributions to the Power and Energy Characteristics of Electrolytic Manganese Dioxide for Electrochemical Capacitors*. Journal of The Electrochemical Society, 2016. 163(6): p. A888-A897.
40. Dupont, M. F., Forghani, M., Cameron, A. P., and Donne, S. W., *Effect of electrolyte cation on the charge storage mechanism of manganese dioxide for electrochemical capacitors*. Electrochimica Acta, 2018. 271: p. 337-350.
41. Dupont, M.F. and S.W. Donne, *Separating Faradaic and Non-Faradaic Charge Storage Contributions in Activated Carbon Electrochemical Capacitors Using Electrochemical Methods: I. Step Potential Electrochemical Spectroscopy*. Journal of the Electrochemical Society, 2015. 162(7): p. A1246-A1254.
42. Dupont, M.F. and S.W. Donne, *Separating the Faradaic and Non-Faradaic Contributions to the Total Capacitance for Different Manganese Dioxide Phases*. Journal of The Electrochemical Society, 2015. 162(5): p. A5096-A5105.

43. Forghani, M. and S.W. Donne, *Method comparison for deconvoluting capacitive and pseudo-capacitive contributions to electrochemical capacitor electrode behavior*. Journal of The Electrochemical Society, 2018. 165(3): p. A664-A673.
44. Forghani, M. and S.W. Donne, *Duty Cycle Effects on the Step Potential Electrochemical Spectroscopy (SPECES) Analysis of the Aqueous Manganese Dioxide Electrode*. Journal of The Electrochemical Society, 2018. 165(3): p. A593-A602.
45. Forghani, M., Mavroudis, H., McCarthy, J., and Donne, S. W., *Electroanalytical characterization of electrochemical capacitor systems using step potential electrochemical spectroscopy*. 2020. Electrochimica Acta, 332: p. 135508.
46. Forghani, M., McCarthy, J., and Donne, S. W., *Oscillatory Current Behavior in Energy Storage Electrode Materials*. 2019. 166(15): p. A3620.
47. Allen J. Bard and L.R. Faulkner, *Electrochemical Methodes : Fundamentals and Applications* SECOND EDITION ed. 2001: John Wiley & Sons.
48. Forghani, M., McCarthy, J., Mavroudis, H., and Donne, S. W., *Electroanalytical Characterization of Electrochemical Capacitor Systems*. Electrochimica Acta, 327, 2019: p. 135010.
49. Forghani, M. and S.W. Donne, *Modification of the Step Potential Electrochemical Spectroscopy Analysis Protocol to Improve Outcomes*. Journal of The Electrochemical Society, 2019. 166(13): p. A2727-A2735.

List of Tables:

Table 1. Specifications of prototype small pouch cells (SPC) and a big pouch cell (BPC).

Table 2. The results of the GCD test with a constant current of 1 A at the potential window of 0 to 2.7 V.

Table 3. Effect of 200 hours float test on capacitance and ESR.

Table 1. Specifications of prototype small pouch cells (SPC) and a big pouch cell (BPC).

Pouch Cell	Cathode Electrode W x H (mm x mm)	Anode Electrode W x H (mm x mm)	Mass of AC (g)	Electrode Layer Number
SPC 1	45 x 58	43 x 56	3.15	14
SPC 2	45 x 58	43 x 56	4.50	20
BPC1-4	50 x 70	48.5 x 68.5	4.46	14

Table 2. The results of the GCD test with a constant current of 1 A at the potential window of 0 to 2.7 V.

Pouch Cell	Capacitance (F)	ESR (mΩ)
SPC 1	82.77	8.8
SPC 2	119.23	7.1
BPC1	116.57	8.4

Table 3. Effect of 200 hours float test on capacitance and ESR.

Pouch Cell	Pre-Float Test		Post-Float Test			
	Capacitance (F)	ESR (mΩ)	Capacitance (F)	Capacitance Change (%)	ESR (mΩ)	ESR Change (%)
BPC 2	120.34	7.64	115.93	-3.66	8.58	+12.30
BPC 3	119.73	7.72	115.56	-3.49	8.44	+9.39
BPC 4	105.06	9.48	100.00	-4.81	10.49	+10.65

List of Figures:

Figure 1. The rate behaviour of the prototype pouch cells.

Figure 2. The Ragone plot for the prototype pouch cells.

Figure 3. A current data for the step potential electrochemical spectroscopy (SPECS) experiment for the small pouch cell 1 (SPC1). (a) Potential and current as a function of time; (b) example of an i - t transient with deconvolution (anodic step of 30 mV to 1.35 V).

Figure 4. Outcomes from a SPECS analysis of the small pouch cell 1 (SPC1). (a) geometric capacitance and resistance values; (b) porous capacitance and resistance values; (c) geometric and porous time constants; and (d) diffusional parameter and residual current.

Figure 5. Cyclic voltammetry and predicted voltammograms based on SPECS data for big pouch cell1 (BPC 1) at $25 \text{ mV}\cdot\text{s}^{-1}$.

Figure 6. (a) Performance of each component as a function of sweep rate; and (b) percentage contribution of each component to the overall capacitance for small pouch cell 1 (SPC1). (c) Performance; and (d) percentage contributions for small pouch cell 2 (SPC2). (e) Performance; and (f) percentage contributions for the big pouch cell 1 (BPC 1).

Figure 7. Outcomes from a SPECS analysis of the big pouch cell 2 (BPC2) pre-float and post-float test. (a) geometric time constant; (b) porous time constant; (c) diffusional parameter; and (d) residual current.

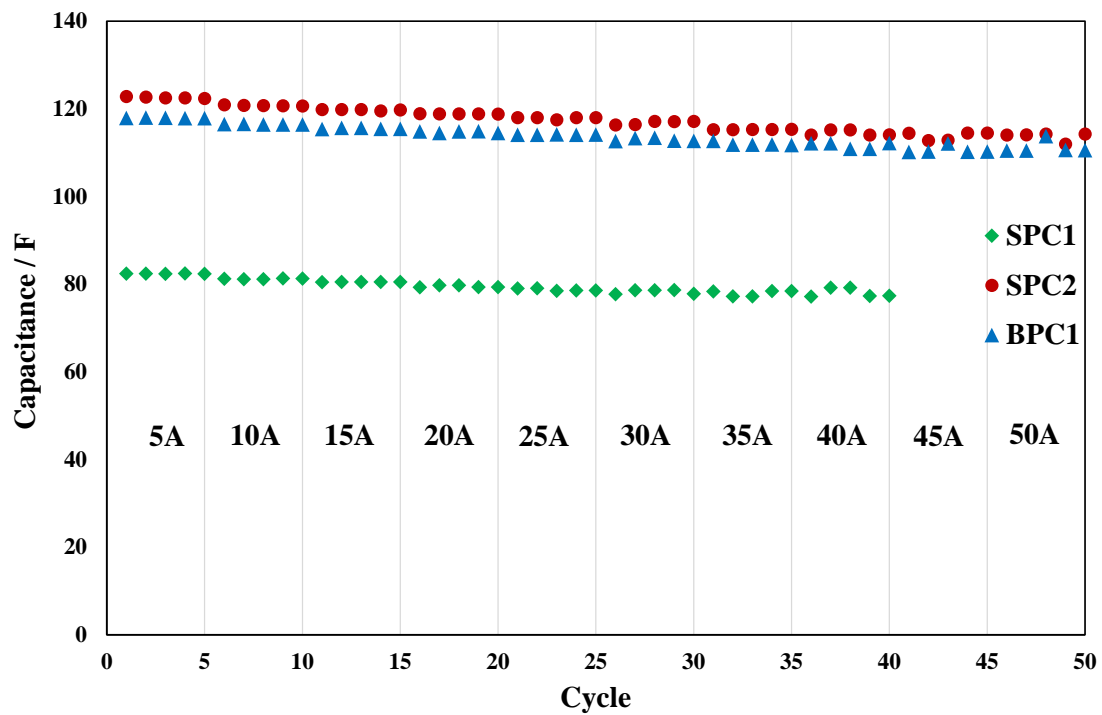


Figure 1. The rate behaviour of the prototype pouch cells.

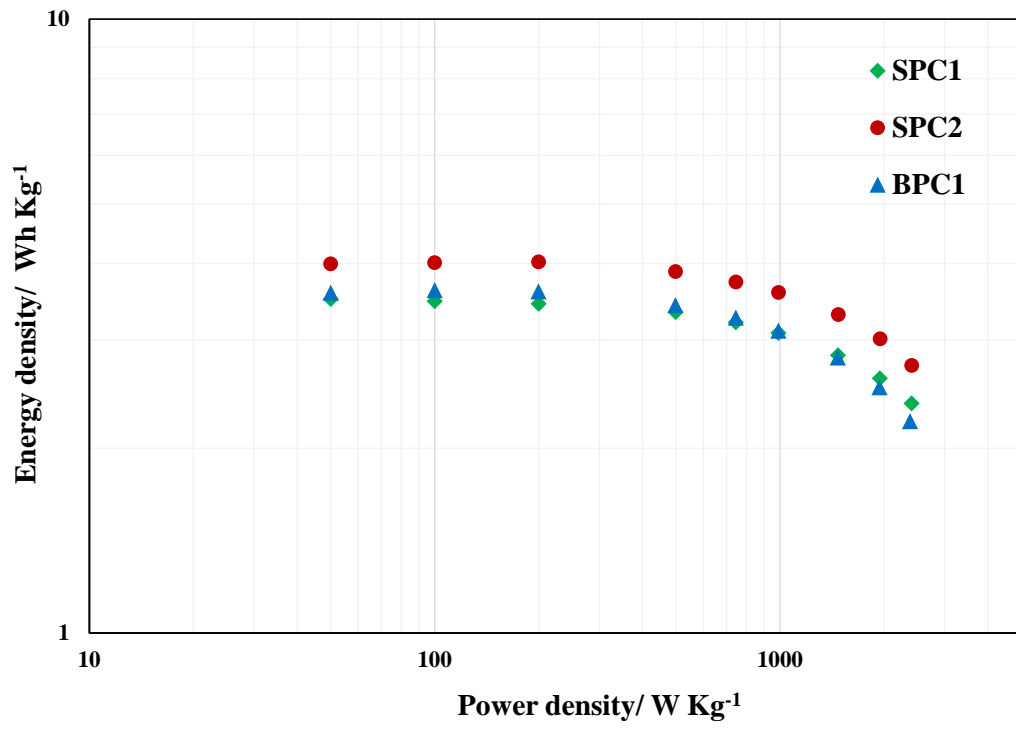


Figure 2. The Ragone plot for the prototype pouch cells.

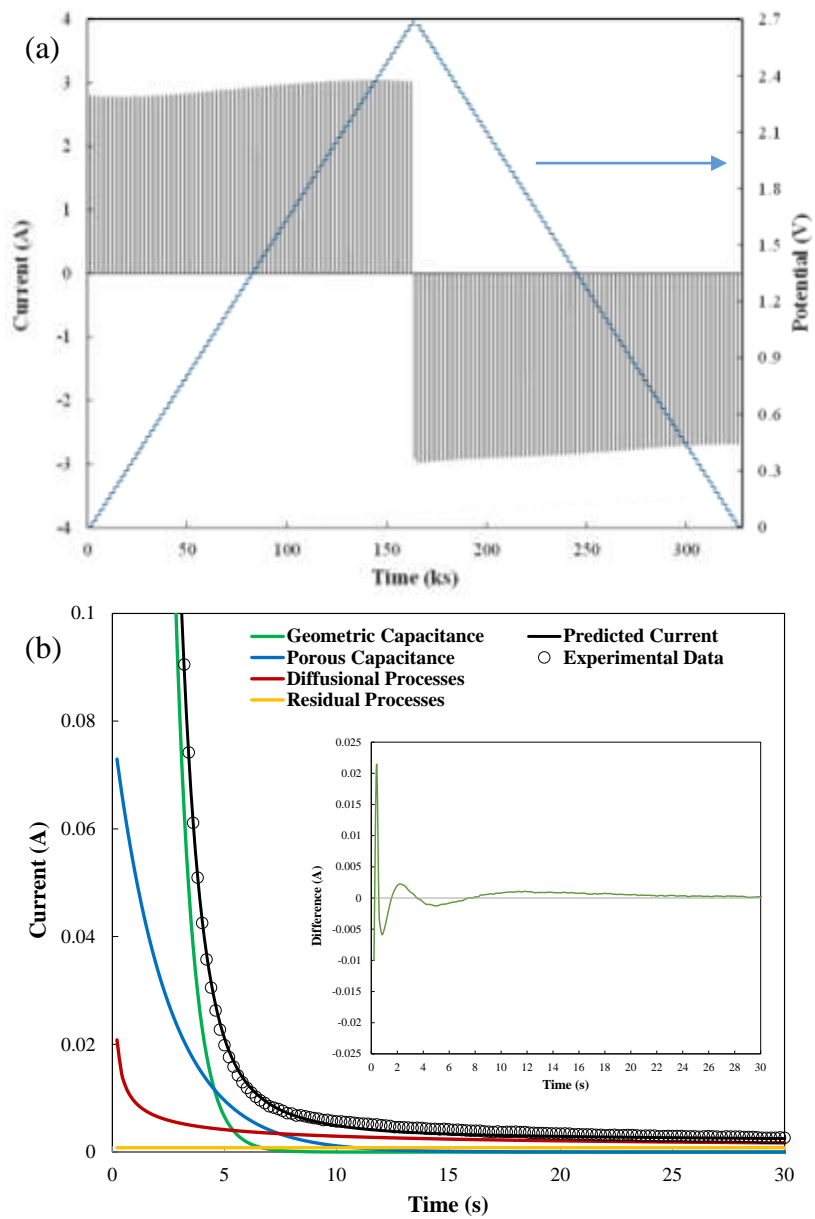


Figure 3. A current data for the step potential electrochemical spectroscopy (SPECS) experiment for the small pouch cell 1 (SPC1). (a) Potential and current as a function of time; (b) example of an i - t transient with deconvolution (anodic step of 30 mV to 1.35 V).

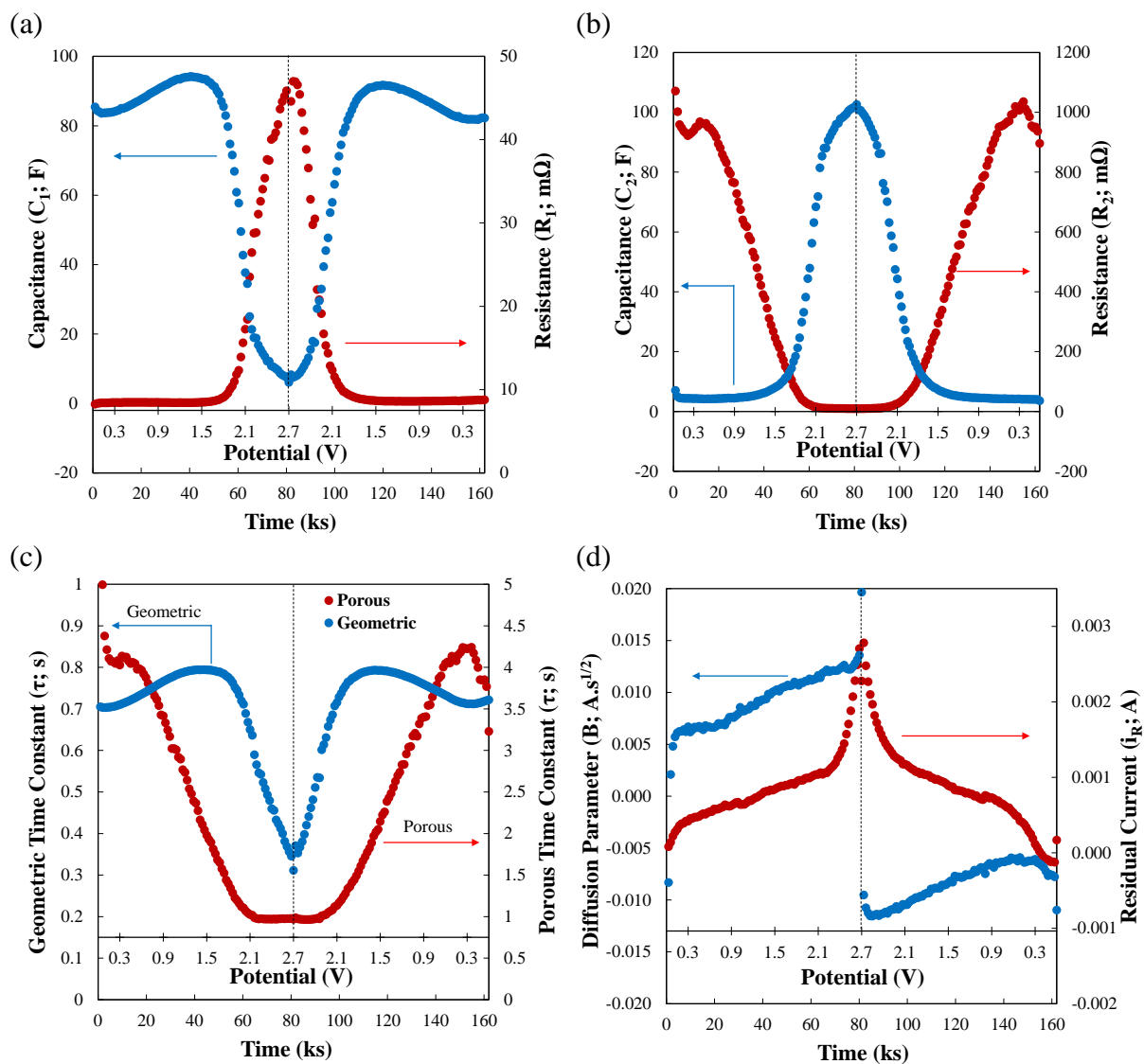


Figure 4. Outcomes from a SPECS analysis of the small pouch cell 1 (SPC1). (a) geometric capacitance and resistance values; (b) porous capacitance and resistance values; (c) geometric and porous time constants; and (d) diffusional parameter and residual current.

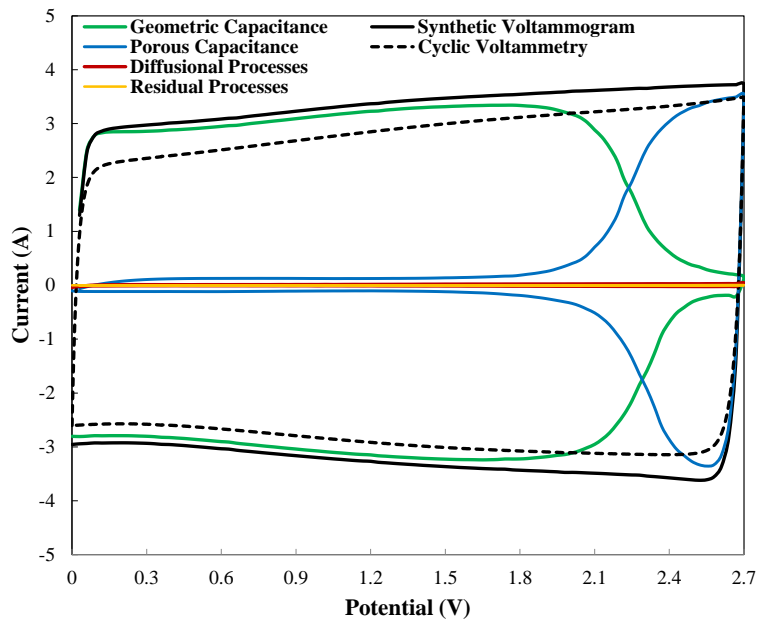


Figure 5. Cyclic voltammogram and predicted voltammograms based on SPECS data for big pouch cell 1 (BPC1) at $25 \text{ mV}\cdot\text{s}^{-1}$.

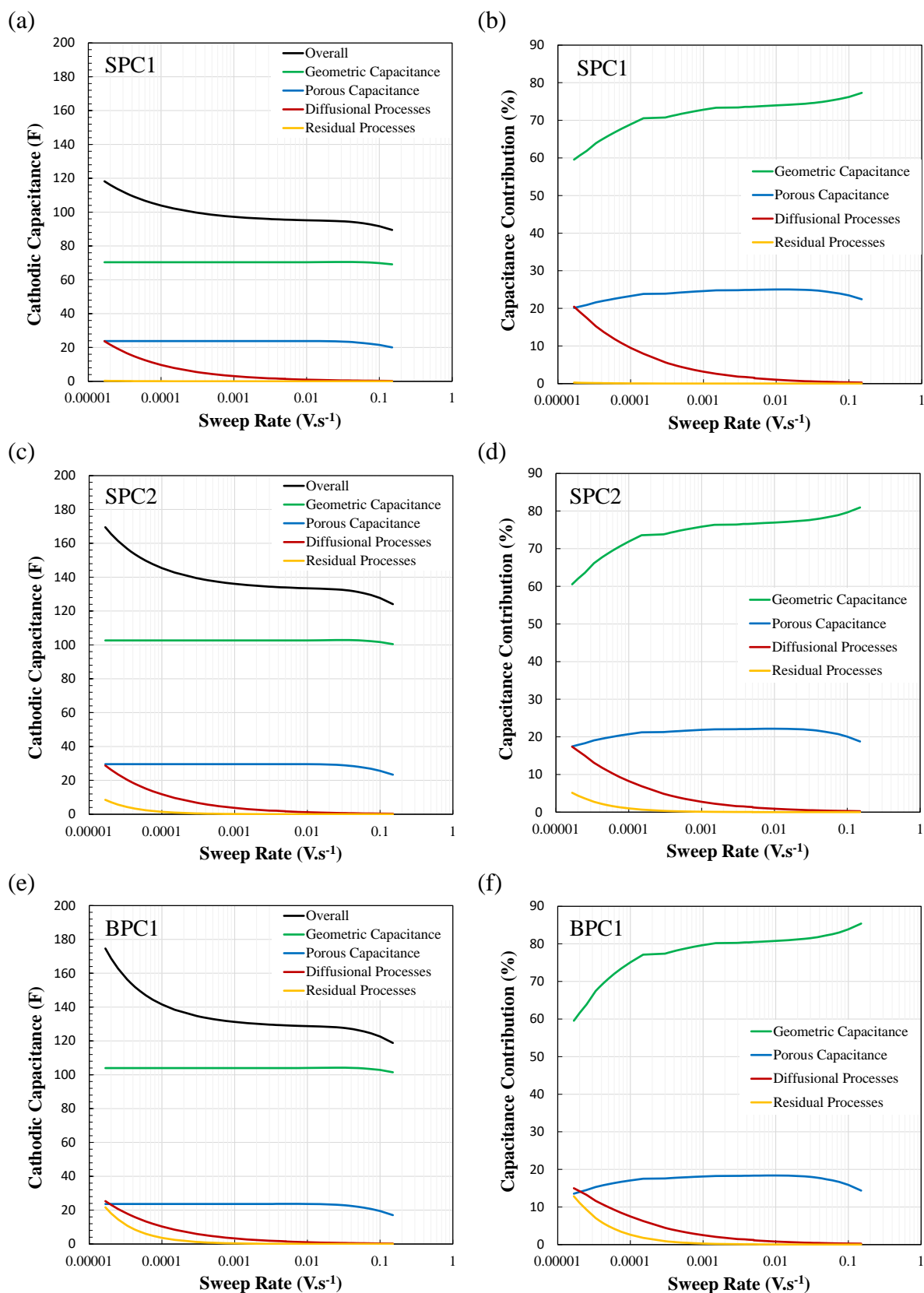


Figure 6. (a) Performance of each component as a function of sweep rate; and (b) percentage contribution of each component to the overall capacitance for small pouch cell 1 (SPC1). (c) Performance; and (d) percentage contributions for small pouch cell 2 (SPC2). (e) Performance; and (f) percentage contributions for the big pouch cell 1 (BPC 1).

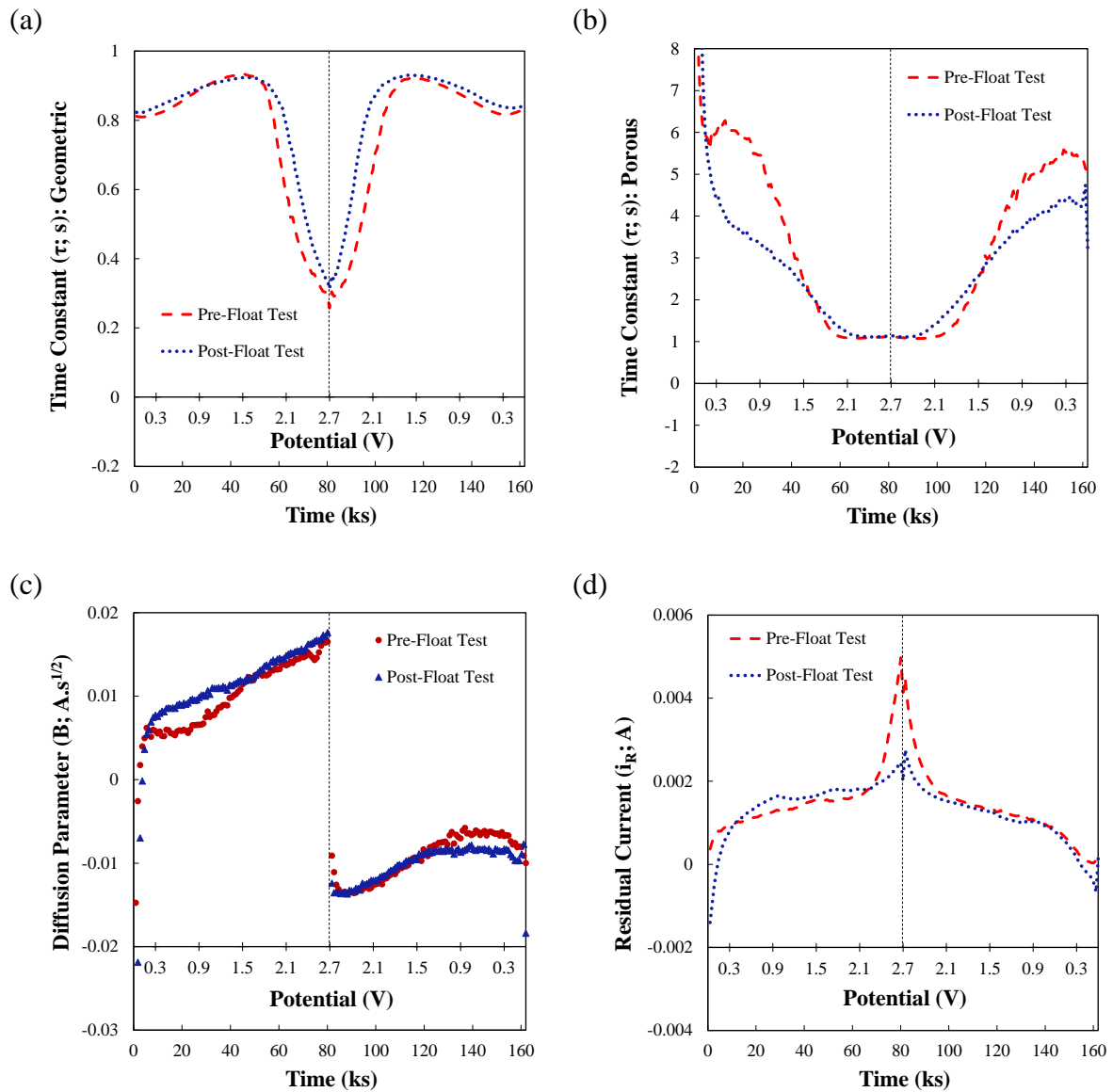


Figure 7. Outcomes from a SPECS analysis of the big pouch cell 2 (BPC2) pre-float and post-float test. (a) geometric time constant; (b) porous time constant; (c) diffusional parameter; and (d) residual current.